ELSEVIER

Chemical Engineering Journal 88 (2002) 59–69

Chemical Engineering Journal

www.elsevier.com/locate/cej

Hydrodynamics and mass transfer in heterogeneous distillation with sieve tray column

H.R. Mortaheb [a], H. Kosuge [a,*], K. Asano [b]

[a] *Department of Chemical Engineering, Graduate School of Science and Engineering, Tokyo Institute of Technology, 2-12-1 O-okayama, Meguro-ku, Tokyo 152-8552, Japan*

[b] *Department of Applied Chemistry, Utsunomiya University, Yoto 7-1-2, Utsunomiya 321-8585, Japan*

Received 23 May 2001; received in revised form 14 September 2001; accepted 15 October 2001

Abstract

Hydrodynamics and separation performance of a sieve tray column in heterogeneous distillation are studied experimentally under total reflux conditions. A correlation for clear liquid height in the heterogeneous liquid region is obtained by modifying the correlation of the homogeneous systems. The volumetric dimensionless diffusion fluxes in the heterogeneous liquid region are smaller than those in the homogeneous liquid region. This may be due to the mass transfer resistance in the liquid phases.

In order to examine the effect of liquid-phase resistance on separation performance, a simulation is carried out by either considering or neglecting the liquid-phase resistance. The simulation shows that the liquid-phase resistance affects the vapor-phase concentration driving forces, volumetric diffusion fluxes and convective mass flux in the heterogeneous liquid region. It also shows that the predicted top vapor concentrations and flow rate are in reasonable agreement with the experimental data in the heterogeneous liquid region by considering the liquid-phase mass transfer resistance.

Keywords: Heterogeneous distillation; Sieve tray; Clear liquid height; Diffusion flux; Liquid-phase resistance

1. Introduction

Heterogeneous distillation is involved in several industrial processes. Steam distillation and heterogeneous azeotropic distillation, which is used for separation of mixtures that are hardly separated by conventional distillation methods, are two examples of the heterogeneous distillation processes. To predict the separation performance of a heterogeneous distillation column, several different algorithms have been proposed to solve the well-known MESH equations, which are the basic equations of the equilibrium stage models. The performance of an actual tray may be predicted by combining appropriate tray efficiencies with these equilibrium stage models. However, there are no reliable estimation methods for stage efficiencies in the highly non-ideal three-phase systems. This made the equilibrium stage models unable to predict the actual tray performance of a heterogeneous distillation column. Alternatively, an intensive non-equilibrium rate-based model can predict the separation performance of actual trays in a heterogeneous distillation column. The model is based on mass transfer equations, which requires sufficient knowledge about the fluid behavior of vapor and both liquid phases. However, quite few experimental works have been done in the heterogeneous distillation [1–4], and sufficient information about behavior of vapor and liquid phases on the tray is not available. Therefore, to solve the mass transfer equations in the rate-based model, several assumptions should be made [5].

Our previous works [6,7] indicate that mass transfer rates can well be correlated in terms of volumetric diffusion fluxes. The obtained correlation for the volumetric diffusion fluxes was successfully used to predict the separation performance of a sieve tray column in the homogeneous distillation. In the present work, the hydrodynamics and mass transfer rates in heterogeneous distillation with the sieve tray column are studied. A similar procedure as applied for the homogeneous systems is used to develop a new prediction method for separation performance in the heterogeneous distillation column.

2. Experimental apparatus and procedures

2.1. Experimental apparatus

A schematic diagram of the setup used in the experiments is shown in Fig. 1. The test section is a 55 mm i.d. tray

* Corresponding author. Tel.: +81-3-5734-2151; fax: +81-3-5734-2151.
E-mail address: hkosuge@chemeng.titech.ac.jp (H. Kosuge).

1385-8947/02/$ – see front matter © 2002 Elsevier Science B.V. All rights reserved.
PII: S1385-8947(01)00263-7

Nomenclature

a	interfacial area per unit volume of liquid on tray (m^{-1})
A_b	bubbling area of tray (m^2)
A_h	total area of holes (m^2)
c_p	specific heat ($J\,kg^{-1}\,K^{-1}$)
d_H	hole diameter (m)
D_{im}	effective diffusion coefficient of component i ($m^2\,s^{-1}$)
F	free area of tray, A_h/A_b
F_a	vapor-phase F-factor, $U_a\rho_G^{0.5}$ ($kg^{0.5}\,m^{-0.5}\,s^{-1}$)
Fr	Froude number, $U_a^2 g^{-1} H_L^{-1}$
g	acceleration due to gravity ($m\,s^{-2}$)
h_L	liquid-phase heat transfer coefficient ($W\,m^{-2}\,K^{-1}$)
H_L	clear liquid height on tray (m)
H_L^{aq}	clear liquid height of aqueous phase on tray (mm)
H_L^{org}	clear liquid height of organic phase on tray (mm)
H_W	weir height (m)
J	diffusion flux ($kg\,m^{-2}\,s^{-1}$)
k_L	liquid-phase mass transfer coefficient ($m\,s^{-1}$)
L	liquid mass flow rate ($kg\,s^{-1}$)
M	mean molecular weight based on overall liquid concentrations in segment ($kg\,mol^{-1}$)
M^I	mean molecular weight of liquid I in segment ($kg\,mol^{-1}$)
N	mass flux ($kg\,m^{-2}\,s^{-1}$)
Nu	vapor-phase Nusselt number
Pr_{Gs}	vapor-phase Prandtl number, $c_{pGs}\mu_{Gs}/\kappa_{Gs}$
q	sensible heat flux ($W\,m^{-2}$)
q_w	wall heat flux ($W\,m^{-2}$)
Re_G	vapor-phase Reynolds number based on vapor velocity at hole, $\rho_G U_h d_H/\mu_G$
Sc_{Gis}	Schmidt number of component i, $\mu_{Gs}/\rho_{Gs}D_{Gim}$
Sh_{Gi}	Sherwood number, $N_{Gi}d_H/\rho_{Gs}D_{Gim}\,\Delta\omega_{Gim}$
T	temperature (K)
U_a	vapor velocity base on bubbling area ($m\,s^{-1}$)
U_h	vapor velocity at hole ($m\,s^{-1}$)
V	vapor mass flow rate ($kg\,s^{-1}$)
We	Weber number, $\rho_G U_a^2 d_H/\sigma$
x	liquid-phase mole fraction
y	vapor-phase mole fraction
z	segment height (m)
z^I	height of liquid I in segment (m)
z^{II}	height of liquid II in segment (m)

Greek letters

α	thermal diffusivity, $\kappa_L/\rho_L c_{pL}$ ($m^2\,s^{-1}$)
β	fraction of liquid I in total liquid in segment, on mole basis, calculated from liquid–liquid equilibrium
β_m	fraction of liquid I in total liquid in segment, on mass basis
β_m^{aq}	fraction of aqueous phase in two-liquid mixture on tray, on mass basis
β_v	fraction of liquid I in total liquid in segment, on volume basis
κ	thermal conductivity ($W\,m^{-1}\,K^{-1}$)
λ	latent heat of vaporization ($J\,kg^{-1}$)
μ	viscosity (Pa s)
ν_s	normal component of interfacial velocity ($m\,s^{-1}$)
ρ	density ($kg\,m^{-3}$)
σ	liquid surface tension ($N\,m^{-1}$)
ω	mass fraction
$\Delta\omega$	mass fraction concentration driving force
$\Delta\omega_{Gim}$	logarithmic mean of top and bottom vapor-phase concentration driving forces, $[(\omega_{Gist}-\omega_{Git})-(\omega_{Gisb}-\omega_{Gib})]/\ln[(\omega_{Gist}-\omega_{Git})/(\omega_{Gisb}-\omega_{Gib})]$

Subscripts

A	most volatile component (ethanol)
b	bottom condition
B	intermediate component (benzene)
cal	calculated value
G	vapor phase
i	component i
L	liquid phase
m	mass fraction average
obs	observed value
s	vapor–liquid interface
t	top condition
∞	bulk condition

Superscripts

I	liquid phase I
II	liquid phase II

column having one sieve tray with 1.5 mm holes. Five different sieve trays are used in this study with a range of 15–30 mm weir height and 1.4–2.8% free area. To generate vapor mixtures with a wide range of concentration in the bottom, the column is equipped with two stills into which the aqueous and organic reflux liquids are fed separately. The reflux liquids are separated into aqueous and organic phases by two decanters at the top and bottom of the column for measuring their concentrations and flow rates. More details about the apparatus are described elsewhere [6].

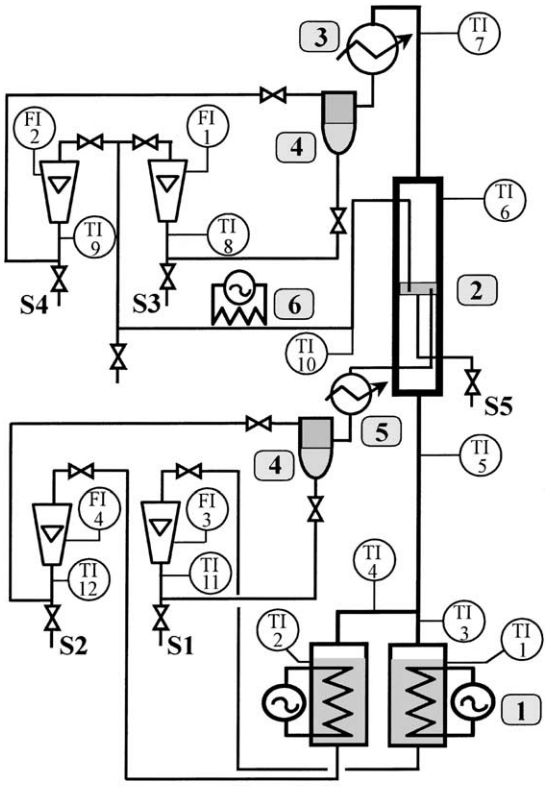

Fig. 1. Schematic diagram of the experimental setup.

2.2. Measurements

The flow rates of aqueous and organic reflux liquids at the top and bottom of the column are measured by precision rotameters at the steady state operation of the column. The concentrations of each liquid phase in the top and bottom reflux liquids are then analyzed by gas chromatograph. The tray holdup is totally drawn and separated in a decanter to measure the weight and concentrations of both liquids on the tray. The clear liquid height of each liquid phase is then obtained from the measured weight and the calculated density of each liquid and the active area of the tray. Since the concentrations and fraction of each liquid phase in the two-liquid sample may change from those on the tray due to decrease in temperature of the sample compared with the tray temperature, the procedure from drawing the tray liquid up to separating the liquid phases in the decanter is carried out in a short time. The vapor-phase volumetric mass flux of each component, $N_{Gi}a$, is obtained by

$$N_{Gi}a = \frac{L_t\omega_{Lit} - L_b\omega_{Lib}}{A_b H_L} \quad (1)$$

where L_t and L_b are the overall reflux flow rates at the top and bottom, respectively, and ω_{Lit} and ω_{Lib} are the overall concentrations of the top and bottom reflux liquids, respectively. The overall vapor-phase volumetric diffusion flux of each component, $J_{Gis}a$, is calculated from the following equation:

$$J_{Gis}a = N_{Gi}a - \left(\sum_{j=1}^{3} N_{Gj}a\right)\omega_{Gis} \quad (2)$$

where ω_{Gis} is the vapor-phase concentration at the vapor–liquid interface, and the vapor concentration in equilibrium with the overall liquid bulk concentration is used as the value of ω_{Gis}. The dimensionless vapor-phase diffusion flux in the heterogeneous liquid region is calculated by

$$Sh_{Gi}\, a\left(\frac{J_{Gis}}{N_{Gi}}\right) d_H = \frac{J_{Gis} a d_H^2}{\rho_{Gs} D_{Gim}\, \Delta\omega_{Gim}} \quad (3)$$

$\Delta\omega_{Gim}$ in the above equation is the logarithmic mean of top and bottom vapor-phase concentration driving forces, in which the vapor concentrations in equilibrium with the overall liquid concentrations are used as the interfacial vapor-phase concentrations at the top and bottom, ω_{Gist} and ω_{Gisb}, respectively.

2.3. Vapor–liquid and vapor–liquid–liquid equilibrium and physical properties

The vapor–liquid and vapor–liquid–liquid equilibriums of the system are estimated from the vapor pressures of pure components by the Antoine equation, and from the liquid-phase activity coefficients by the UNIQUAC equation, where the Antoine constants and UNIQUAC parameters are taken from [8]. The viscosity of the pure vapor is calculated from Chung et al. method and for vapor mixture Wilke's method is applied. The thermal conductivity of vapor and liquid mixtures are calculated using the methods of Chung et al. and Li, respectively. The surface tension of liquid mixture is calculated using the modified Macleod correlation. The vapor-phase binary diffusion coefficient is estimated by the correlation of Fuller et al., and for estimation of the effective diffusion coefficients in the liquid phase the Perkins and Geankoplis equation is used [9].

2.4. Range of experimental variables

Total reflux distillation runs under atmospheric pressure were made in the heterogeneous liquid region of the ethanol–benzene–water system by varying vapor flow rates and bottom concentrations. The concentration regions of distillation runs are shown in Fig. 2, where the tip and tale of the arrows represent the top and bottom concentrations, respectively. For further discussions, the experimental concentration ranges are grouped into four regions in terms of driving force and physical properties. The whole region is

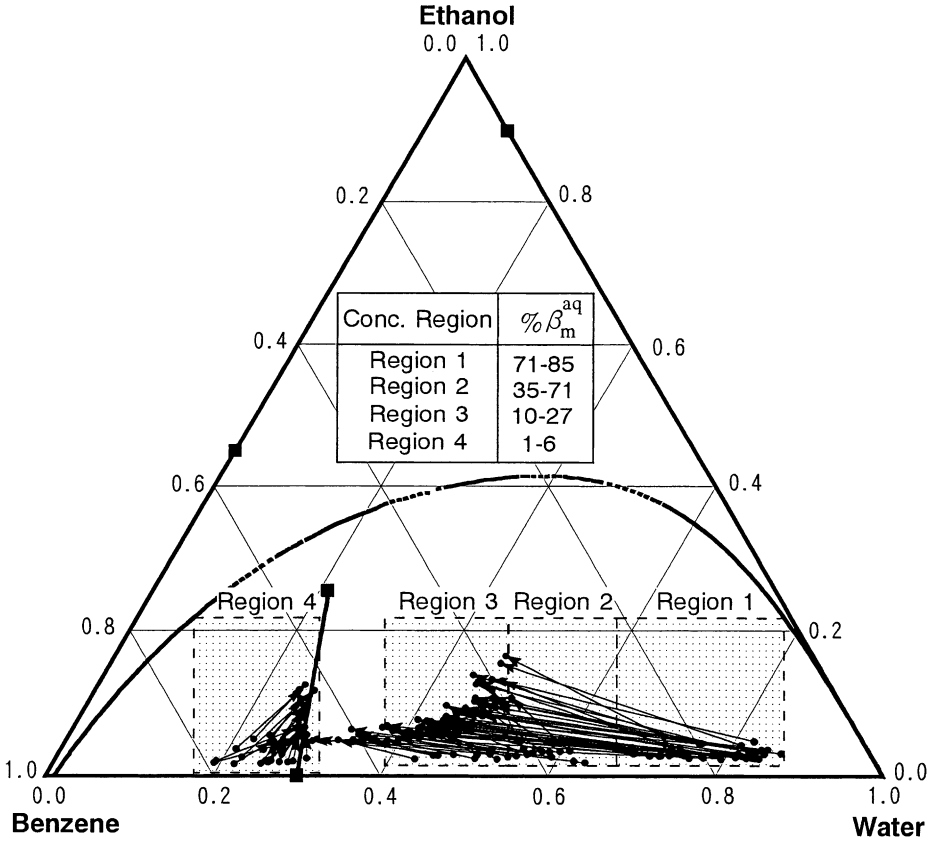

Fig. 2. Concentration regions of experimental runs.

divided from the vapor line because of different tendencies of the driving forces for the benzene and water in the two sides of the vapor line. Region 3 is separated from the other regions in the right-hand side of the vapor line in terms of difference in the vapor density, which is mentioned in Section 3.1. The remained region is split into regions 1 and 2 because of large driving forces and therefore long distillation paths of benzene and water in region 1.

3. Experimental results

3.1. Clear liquid height in heterogeneous liquid region

Froth regime was observed on the tray in all distillation runs. The observed clear liquid heights on the tray are shown in Fig. 3. The solid line in the figure represents the previous correlation for the froth regime in the homogeneous liquid region, obtained for the acetone–methanol–ethanol, ethanol–benzene and ethanol–benzene–water systems [6,7]. The observed data of clear liquid height show similar tendencies with the vapor-phase Reynolds number. However, their values are different with the concentration regions, that is, the observed data of regions 1 and 2 show lower values than the previous correlation, while those of regions 3 and 4 agree with the correlation. The difference between the correlation and the observed values of regions 1 and 2 may be caused by the physical properties and/or the volumetric ratio of two liquids, which characterizes the two-liquid conditions on the tray. Among the physical properties, the vapor density varies

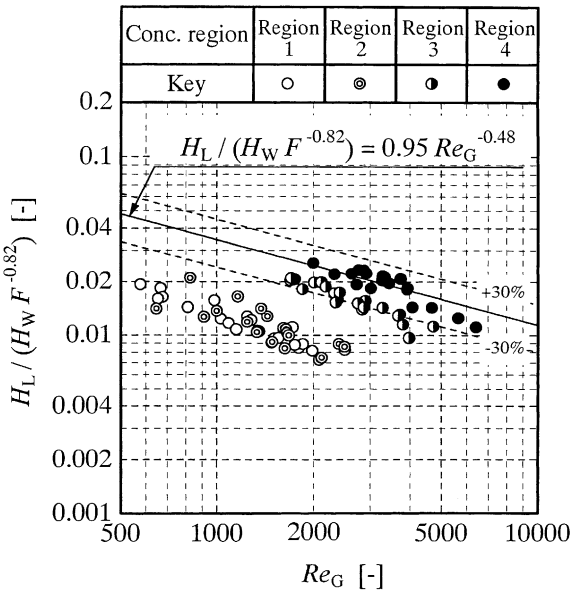

Fig. 3. Effect of vapor-phase Reynolds number on clear liquid height in heterogeneous liquid region.

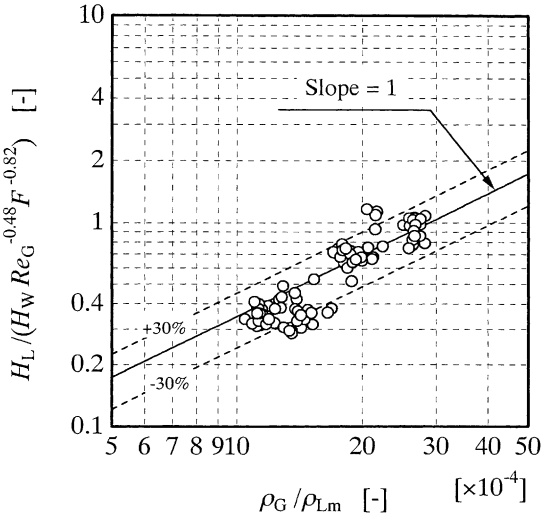

Fig. 4. Effect of vapor density on clear liquid height in heterogeneous liquid region.

widely within the present concentration regions while the variation range of vapor density was narrow in the previous experiments [6,7]. Then, the observed clear liquid heights are plotted against the vapor density in Fig. 4. The abscissa in the figure, ρ_G/ρ_{Lm}, is a normalized vapor density with the average of liquid densities based on the mass fractions of aqueous and organic phases. As shown in the figure, the clear liquid height increases by increasing ρ_G/ρ_{Lm} with a slope of 1. On the other hand, the effect of volumetric ratio of two liquids on the clear liquid height was found to be negligible, as mentioned also by Herron et al. [3].

Fig. 5 shows the final correlation for clear liquid height in the heterogeneous liquid region. For comparison, the

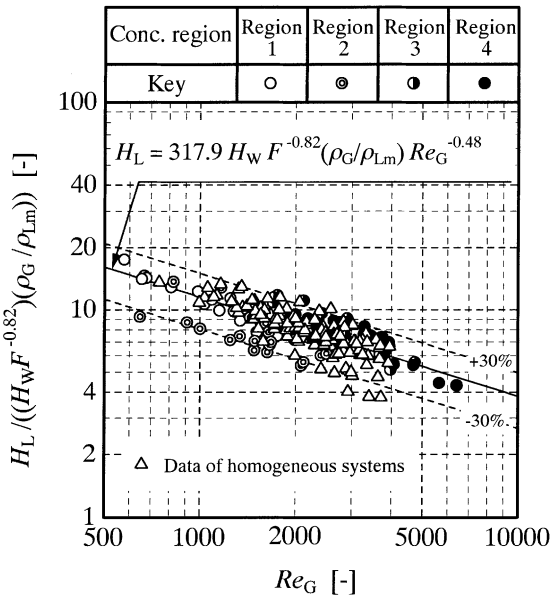

Fig. 5. Clear liquid height in heterogeneous liquid region.

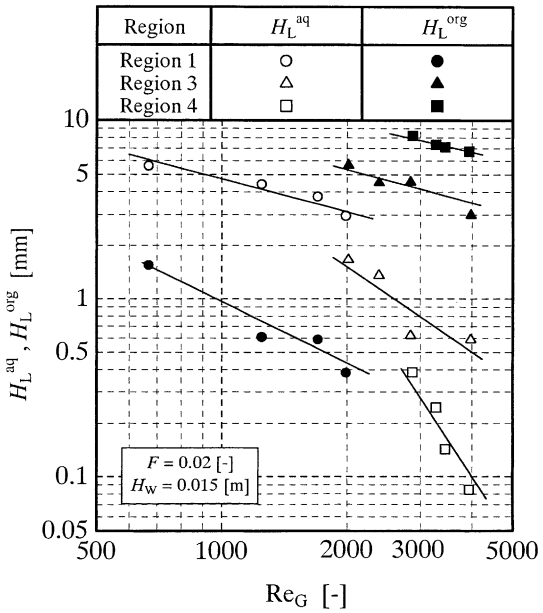

Fig. 6. Clear liquid heights of aqueous and organic phases in heterogeneous liquid region.

experimental data of clear liquid height in the homogeneous liquid region for the acetone–methanol–ethanol, ethanol–benzene and ethanol–benzene–water systems [6,7] are also shown. The clear liquid height in the froth regime for both heterogeneous and homogeneous liquid regions is well correlated by Eq. (4).

$$H_L = 317.9 H_W F^{-0.82} \left(\frac{\rho_G}{\rho_{Lm}}\right) Re_G^{-0.48} \quad (4)$$

This implies that the bubbles and dispersed droplets are well mixed with the continuous liquid, and both liquids flow out constantly from the tray. This is also confirmed by the observation of fluid behavior on the tray, that is, the fluid on the tray is a cloudy emulsion in which continuous and dispersed phases are difficult to be distinguished. In order to confirm whether both liquids flow out together from the tray, the observed clear liquid heights of aqueous and organic phases on a tray are plotted in Fig. 6. The figure shows that clear liquid heights for both phases decrease with vapor-phase Reynolds number, and the tendency for the clear liquid heights of both liquids with large values is similar to that for the total clear liquid height. On the other hand, the clear liquid heights with small values show different slopes. This is probably due to the small amount of a liquid, which remains on the surface of the other liquid when two liquids in the decanter are separated from each other. Such error is more significant for the liquid with a small clear liquid height.

3.2. Mass transfer in heterogeneous liquid region

The dimensionless volumetric diffusion fluxes in the heterogeneous liquid region are plotted against vapor-phase

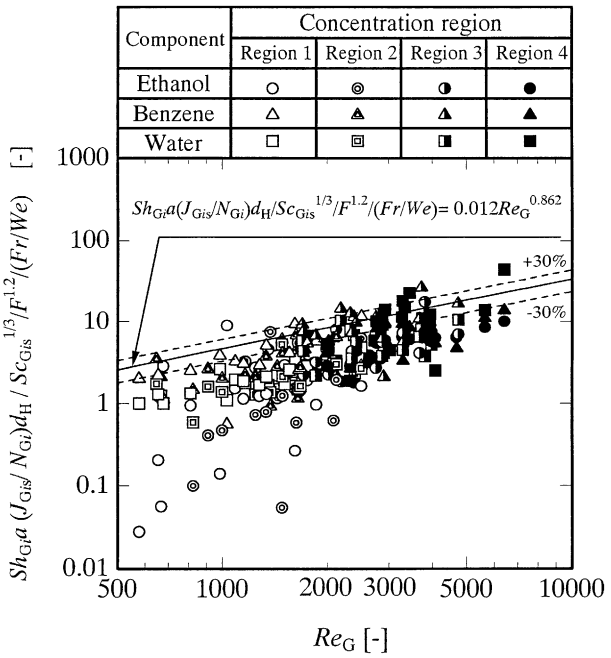

Fig. 7. Plot of dimensionless volumetric diffusion fluxes in heterogeneous liquid region against vapor-phase Reynolds number.

Reynolds number in Fig. 7. The solid line in the figure represents the correlation for the ethanol–benzene and ethanol–benzene–water systems in the homogeneous liquid region [7]. The figure shows that some of the diffusion flux data of ethanol, which were obtained in regions 1 and 2, are scattered. This is due to small concentration driving force and diffusion flux for these data, where small concentration change for ethanol along the tray was observed. The tendencies of dimensionless volumetric diffusion fluxes except for the large scattered data in the heterogeneous liquid region agree with the correlation, however, their values are smaller than the correlation. The cause of smaller volumetric diffusion fluxes in the heterogeneous liquid region than those in the homogeneous liquid region, is supposed to be lower mass transfer rate due to the effect of liquid-phase mass transfer resistance. It is discussed more in the following section.

4. Simulation

4.1. Mass transfer at vapor–liquid interfaces

Fig. 8 shows a schematic diagram of heat and mass transfer in the heterogeneous system. If the mass transfer resistances in the liquid phases were neglected, the liquid concentrations at the vapor–liquid interfaces, ω^{I}_{Lis} and ω^{II}_{Lis}, would be same as those in the liquid bulks, that is, $\omega^{I}_{Lis} = \omega^{I}_{Li\infty}$ and $\omega^{II}_{Lis} = \omega^{II}_{Li\infty}$. In addition, if two liquid phases are in equilibrium with each other, the vapor-phase concentrations at both vapor–liquid interfaces, ω^{I}_{Gis} and ω^{II}_{Gis}, coincide on the vapor line.

However, considering the mass transfer resistance in the liquid phases and assuming equilibrium condition between two liquid phases, the liquid concentrations at vapor–liquid interfaces, ω^{I}_{Lis} and ω^{II}_{Lis}, take different values from the liquid bulks concentrations, $\omega^{I}_{Li\infty}$ and $\omega^{II}_{Li\infty}$, respectively. Therefore, the vapor-phase concentrations at the vapor–liquid interfaces, ω^{I}_{Gis} and ω^{II}_{Gis}, and consequently

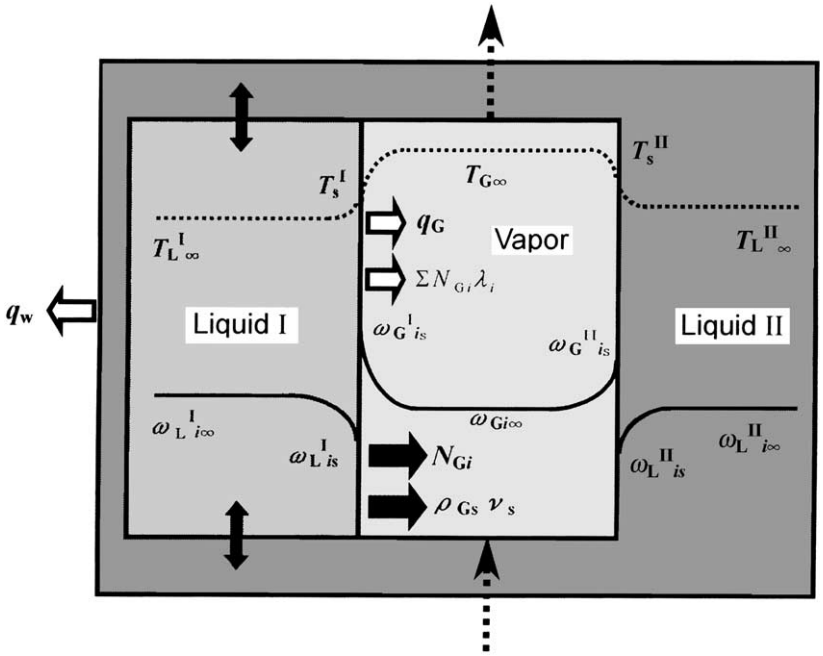

Fig. 8. Schematic diagram of mass and heat transfer in heterogeneous distillation.

the vapor-phase concentration driving forces, $\omega^{I}_{Gis} - \omega_{Gi\infty}$ and $\omega^{II}_{Gis} - \omega_{Gi\infty}$, take different values. The different vapor-phase concentration driving forces, which affect the mass transfer rate from vapor to each liquid phase, may change the overall mass transfer rate. Therefore, the smaller volumetric mass transfer rate in the heterogeneous liquid region, which is shown in Fig. 7, may be caused by the effect of liquid-phase mass transfer resistance. This is confirmed by simulation in the next section.

4.2. Simulation procedure

The separation performance of the heterogeneous distillation column can be simulated by a segment-by-segment method from bottom to top of the liquid on the tray with known bottom overall reflux flow rate and concentrations. The basic equations for simulation are summarized in Table 1. In each segment, the heat and mass transfer rates between the vapor and aqueous phases and between the vapor and organic phases are calculated separately. The dimensionless volumetric diffusion flux correlation obtained for the systems in the homogeneous liquid region (Eq. (5) in Table 1) is applied for calculation of the vapor-phase diffusion fluxes at each vapor–liquid interface. The following assumptions are made in the model. In the present experiments, the concentrations of aqueous and organic liquids on the tray, which are measured after separating in the decanter, are close to the equilibrium. Since the retention time in the decanter is short, the conditions close to the equilibrium may be established on the tray, not in the decanter. Then, the liquid phases on the tray are assumed to be in equilibrium with each other. The overall concentrations at the bottom of the tray are used as initial values for calculation.

Since the liquid flow path length on the tray is short in the present apparatus, change of the liquid concentrations along the horizontal direction might be small. Then, the liquid is assumed to be well mixed in the horizontal direction. However, as the vapor passes through the liquid in plug flow, the mass transfer occurs between the vapor and liquid phases at each point in the vertical direction, and the liquid and vapor concentrations change in this direction. Therefore, the tray liquid is divided into a number of thin horizontal segments in the simulation procedure, and perfect liquid mixing is assumed in each segment.

The steps of the simulation are as follows:

1. Clear liquid height on the tray is calculated by Eq. (4) and is divided into segments with the height of z.
2. The concentrations and flow rate of each liquid phase are calculated from the overall liquid concentrations and flow rate at the inlet of the segment by the liquid–liquid equilibrium calculation.
3. The following steps are carried out separately for each liquid phase:
   - 3.1. The vapor-phase concentrations and temperature at the vapor–liquid interface, ω_{Gis} and T_s, are calculated from the liquid concentrations at the interface by the vapor–liquid equilibrium calculations. As initial values for ω_{Lis}, the liquid bulk concentrations, $\omega_{Li\infty}$, are applied.
   - 3.2. The volumetric vapor-phase diffusion fluxes, $J_{Gis}a$, are calculated from Eq. (5).
   - 3.3. The vapor-phase volumetric convective mass flux, $\rho_{Gs}\nu_s a$, and the volumetric mass fluxes, $N_{Gi}a$, are calculated by Eq. (8) [10] and Eq. (9) in Table 1, respectively, where the equation for the volumetric vapor-phase sensible heat flux (Eq. (6) in Table 1) is derived from the analogy between heat and mass transfer.
   - 3.4. The volumetric liquid-phase diffusion fluxes, $J_{Lis}a$, are calculated by

$$J_{Lis}a = N_{Li}a - \left(\sum_{j=1}^{3} N_{Lj}a\right)\omega_{Lis} \tag{15}$$

$$N_{Li} = N_{Gi} \tag{16}$$

   - 3.5. The new liquid concentrations at the vapor–liquid interface are estimated by applying the Newton–Raphson method with the following objective functions:

$$f_1(\omega_{L2s}, \omega_{L3s}) = \omega_{L2s} - \left(\omega_{L2\infty} - \frac{J_{L2s}a}{\rho_L k_{L2}a}\right) \tag{17A}$$

Table 1
Basic equations for simulation in heterogeneous distillation

Clear liquid height

$$H_L = 317.9 H_W F^{-0.82}\left(\frac{\rho_G}{\rho_{Lm}}\right) Re_G^{-0.48} \tag{4}$$

Mass and heat transfer rates equations

Vapor phase

$$Sh_{Gi}\, a\left(\frac{J_{Gis}}{N_{Gi}}\right) d_H = 0.012 Re_G^{0.862} Sc_{Gis}^{1/3} F^{1.2}\left(\frac{Fr}{We}\right) \tag{5}$$

$$Nu_G\, a d_H = 0.012 Re_G^{0.862} Pr_{Gs}^{1/3} F^{1.2}\left(\frac{Fr}{We}\right) \tag{6}$$

$$q_G a = \frac{Nu_G\, a d_H (T_s - T_\infty)\kappa_{Gs}}{d_H^2} \tag{7}$$

$$\rho_{Gs}\nu_s a = \frac{\sum(-J_{Gis}a\lambda_i) - q_w a - q_G a}{\sum -\lambda_i \omega_{Gis}} \tag{8}$$

$$N_{Gi}a = J_{Gis}a + \rho_{Gs}\nu_s a \omega_{Gis} \tag{9}$$

Liquid phase

$$k_{Li}a = 19\,700 D_{Lim}^{0.5}(0.4F_a + 0.17) \tag{10}$$

$$h_L a = 19\,700\alpha^{0.5}(\rho_L c_{pL})(0.4F_a + 0.17) \tag{11}$$

Overall and component mass balances

$$\Delta V = \sum[(N_{Gi}a)^I z^I + (N_{Gi}a)^{II} z^{II}]A_b \tag{12}$$

$$\Delta(V\omega_{Gi}) = [(N_{Gi}a)^I z^I + (N_{Gi}a)^{II} z^{II}]A_b \tag{13}$$

$$\beta_m = \beta\left(\frac{M^I}{M}\right), \qquad \beta_v = \frac{\beta_m/\rho_L^I}{\beta_m/\rho_L^I + (1-\beta_m)/\rho_L^{II}} \tag{14A}$$

$$z^I = z\beta_v, \qquad z^{II} = z(1-\beta_v) \tag{14B}$$

$$f_2(\omega_{L2s}, \omega_{L3s}) = \omega_{L3s} - \left(\omega_{L3\infty} - \frac{J_{L3s}a}{\rho_L k_{L3}a}\right) \quad (17B)$$

where ω_{L2s} and ω_{L3s} are selected as the independent variables to optimize the objective functions, and the required partial derivatives are obtained numerically. The liquid-phase volumetric mass transfer coefficients, $k_{Li}a$, in the above equations are calculated by Eq. (10) in Table 1 [11].

3.6. For each liquid phase, steps 3.1–3.5 are repeated until convergence is achieved for ω_{Lis}.

4. The liquid bulk temperature is calculated by

$$T_{L\infty} = T_s + \frac{q_L a}{h_L a} \quad (18)$$

where the volumetric liquid-phase heat transfer coefficient, $h_L a$, is obtained from the analogy between heat and mass transfer (Eq. (11) in Table 1). The volumetric liquid-phase heat flux, $q_L a$, is obtained by heat balance around the vapor–liquid interface:

$$q_L a = q_G a - \sum \lambda_i N_{Gi} a \quad (19)$$

5. The overall flow rate and concentrations at the top of the segment are obtained from the overall and component mass balances (Eqs. (12) and (13) in Table 1), where the mass transfer rate of vapor and each liquid phase is assumed to be proportional to the height of that liquid in the segment. The heights of both liquids in the segment are calculated by Eqs. (14A) and (14B) in Table 1, in which the fraction of liquid I in the total liquid, β, is obtained from liquid–liquid equilibrium based on the overall liquid concentrations in the segment.
6. The calculations from steps 2 to 5 are repeated up to the top of the liquid on the tray.

For comparison, simulation by neglecting the liquid-phase resistance is also carried out.

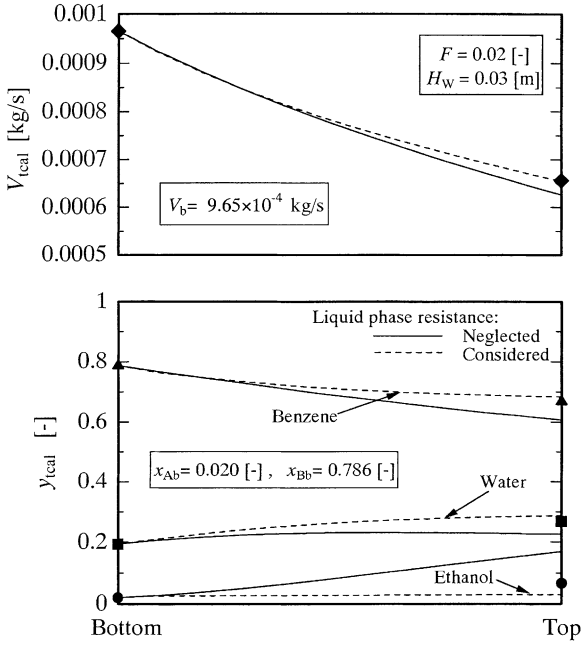

Fig. 9. Predicted axial distributions of top vapor flow rate and concentrations.

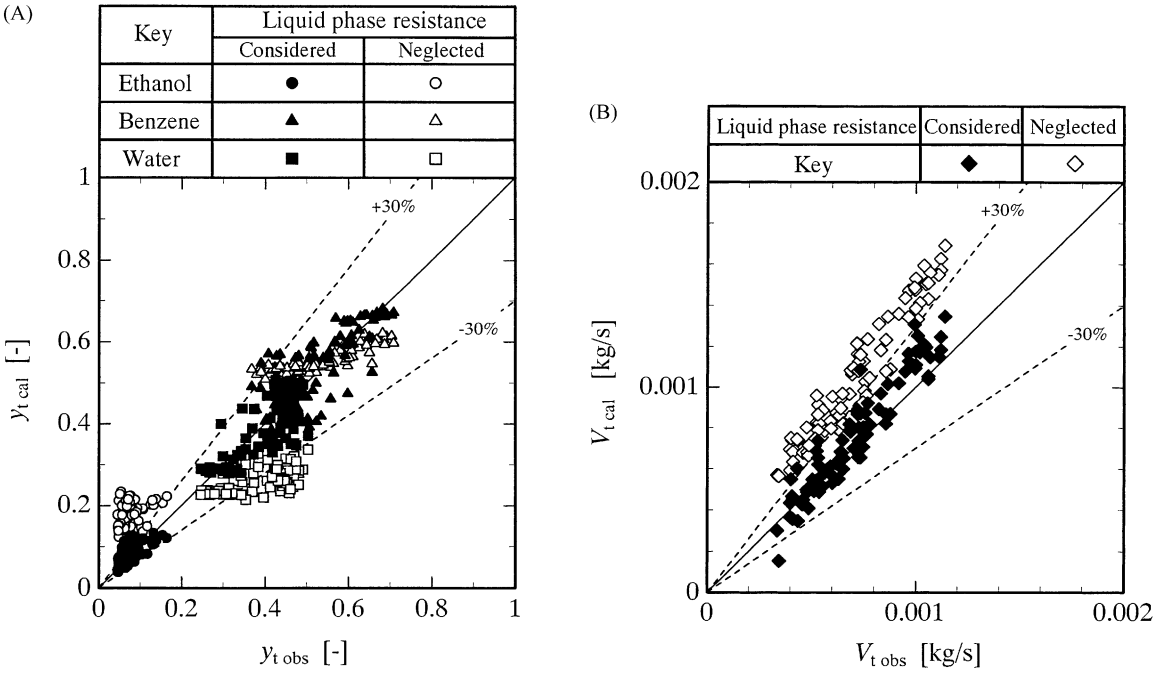

Fig. 10. (A) Comparison between predicted and observed top vapor concentrations. (B) Comparison between predicted and observed top vapor flow rates.

4.3. Simulation results

Fig. 9 shows an example of predicted axial distributions of the vapor flow rate and concentrations, where the calculation conditions are shown in the figure. The filled symbols denote the observed data. The dashed and solid lines represent simulation results by considering liquid-phase resistance and by neglecting it, respectively. As shown in the figure, the predicted values by considering the liquid-phase resistance are in good agreement with the observed data, while the agreement is poor when the resistance is neglected.

The comparison of predicted top vapor concentrations and flow rate with the observed values for all the data are shown in Fig. 10(A) and (B). The filled and open symbols represent the predicted values by considering liquid-phase resistance and by neglecting it, respectively. Both predicted values of top vapor concentrations and flow rate are in better agreement with the observed ones by taking the liquid-phase resistance into account.

5. Discussion

5.1. Effect of liquid-phase resistance on separation performance in heterogeneous liquid region

To explain the difference between simulation results by considering and neglecting liquid-phase resistance, the axial distributions of concentration driving forces at both vapor–liquid interfaces are shown in Fig. 11(A). The calculations were made with the same bottom conditions as those in Fig. 9. As shown in the figure, when the liquid-phase resistance is considered, the profiles of vapor-phase concentration driving force are quite different for aqueous and organic phases. This is due to vapor–liquid equilibrium of the ethanol–benzene–water system, that is, small changes of liquid concentrations at vapor–liquid interfaces from liquid bulks concentrations provide large differences between vapor concentrations at these interfaces.

Fig. 11(B) and (C) show the axial distribution of volumetric diffusion fluxes and convective mass flux, respectively. The volumetric diffusion fluxes and convective mass flux by considering the liquid-phase resistance are smaller than those by neglecting the resistance. These tendencies correspond to the behavior of vapor-phase concentration driving forces.

The effect of liquid-phase mass transfer resistance on concentration driving forces, diffusion fluxes and convective mass flux affects the overall mass transfer rates in the heterogeneous liquid region. To investigate the magnitude of this effect, the dimensionless volumetric diffusion fluxes are calculated using the simulated top overall liquid concentrations and reflux flow rate. The result of calculation is illustrated in Fig. 12. The calculated dimensionless volumetric diffusion fluxes take smaller values than those of the correlation but closer to the observed values, which are

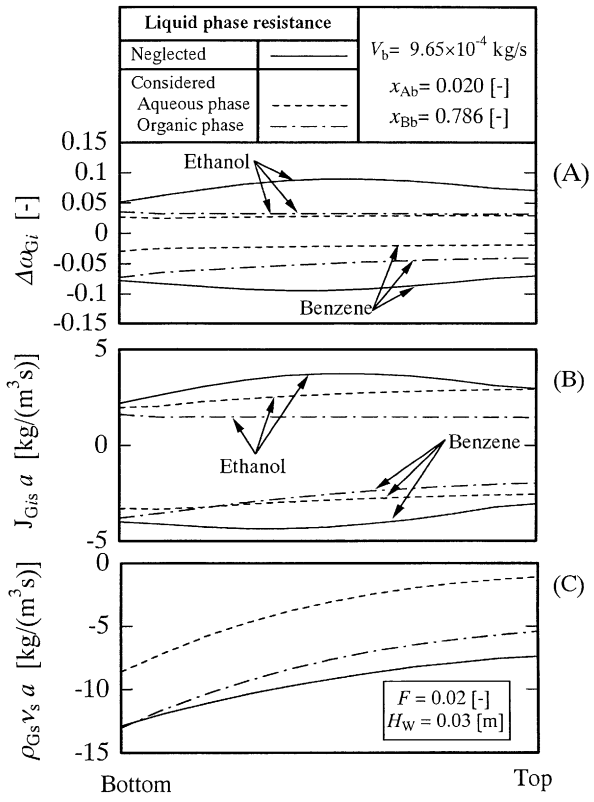

Fig. 11. Axial distributions of (A) concentration driving forces, (B) volumetric diffusion fluxes and (C) volumetric convective mass flux.

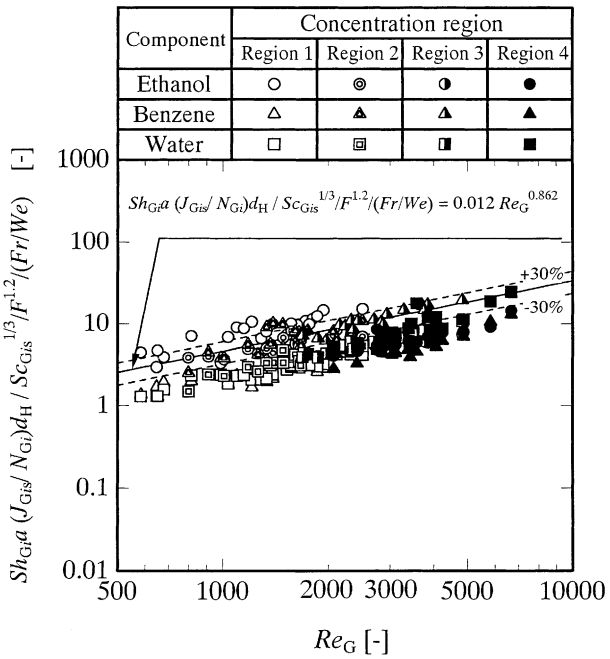

Fig. 12. Calculated dimensionless volumetric diffusion fluxes by simulation results.

shown in Fig. 7. Fig. 12 also indicates that the larger scattering of the observed dimensionless volumetric diffusion fluxes than the calculated ones may be due to the experimental error for measurement of the top and bottom flow rates, and the concentration analysis. It is then concluded that the overall mass transfer rate in the heterogeneous liquid region is smaller than the mass transfer rate of the homogeneous systems mainly due to the effect of liquid-phase resistance.

5.2. Comparison of present mass transfer model with previous models

Since the present model is based on the obtained correlation by a laboratory-scale column, the applicability of the model may be judged by comparing the results with those from other mass transfer models. However, there is currently no experimental model for prediction of mass transfer rate of the heterogeneous systems. Then, the previous models of the homogeneous systems [12–14] are applied for this purpose. The volumetric diffusion fluxes between vapor and each liquid phase on the tray are then estimated from the matrix of binary mass transfer coefficients using the procedure described by Taylor and Krishna [15], where the required binary mass transfer coefficients are calculated by using the previous mass transfer models [12–14]. The liquids on the tray are assumed as two stratified layers, whose clear liquid heights are estimated by prediction of total clear liquid height from Eq. (4) and using the liquid–liquid equilibrium calculations. Fig. 13 shows an example of comparison between the observed top concentrations with the predicted values, where the mass transfer coefficients are estimated by Stichlmair model [12]. For comparison, the predicted values by the present model are also shown. The figure shows a fair agreement of the predicted top concentrations by the Stichlmair model [12] with those by the present model, and with the observed values. Similar results were obtained when the Chan and Fair model [13] was used, whereas applying the Zuiderweg model [14] gave poor results. Since the previous mass transfer models are based on distillation data by various columns, the fair agreement of the predicted values by the previous models with those by the present model might show that the present model is applicable to the columns with different tray specifications, although further examinations are necessary to verify this.

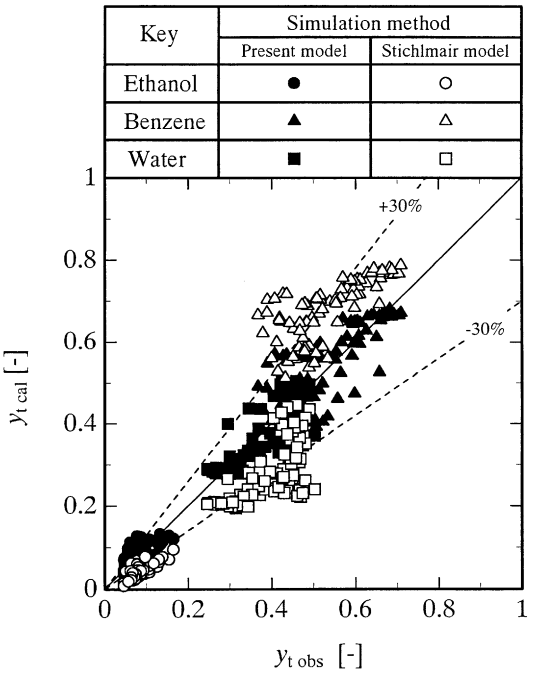

Fig. 13. Comparison of top vapor concentrations predicted by the Stichlmair model [12] and the present model with the observed ones.

6. Conclusions

An experimental study is made on hydrodynamics and mass transfer in the heterogeneous distillation for ethanol–benzene–water system with a sieve tray column. A simulation procedure is proposed to predict the separation performance in the heterogeneous distillation. Based on the results, the following conclusions are obtained:

1. A correlation for clear liquid height in the heterogeneous liquid region is obtained by modifying the correlation of the homogeneous systems.
2. The dimensionless volumetric diffusion fluxes in the heterogeneous liquid region are smaller than those in the homogeneous liquid region. However, this is due to the significant effect of the liquid-phase mass transfer resistance.
3. By considering the liquid-phase resistance, the predicted top vapor concentrations and flow rate agree with the observed ones in the heterogeneous liquid region.

References

[1] N.A. Ashton, A. Arrowsmith, C.J. Yu, Distillation hydraulics with immiscible liquids, IChemE Symp. Ser. 104 (1987) B113–B126.
[2] B. Davies, Z. Ali, K.E. Porter, Distillation of systems containing two liquid phases, AIChE J. 33 (1987) 161–163.
[3] C.C. Herron Jr., B.K. Kruelskie, J.R. Fair, Hydrodynamics and mass transfer on three-phase distillation trays, AIChE J. 34 (1988) 1267–1274.
[4] B.P. Cairns, I.A. Furzer, Multicomponent three-phase azeotropic distillation. I. Extensive experimental data and simulation results, Ind. Eng. Chem. Res. 29 (1990) 1349–1363.
[5] M. Lao, R. Taylor, Modeling mass transfer in three-phase distillation, Ind. Eng. Chem. Res. 33 (1994) 2637–2650.
[6] H.R. Mortaheb, Y. Iimuro, H. Kosuge, K. Asano, Mass transfer in ternary distillation with sieve tray column, J. Chem. Eng. Jpn. 33 (2000) 597–604.
[7] H.R. Mortaheb, H. Kosuge, K. Asano, Mass transfer in foam and froth regimes in distillation with sieve tray column, J. Chem. Eng. Jpn. 34 (2001) 493–500.
[8] J. Gmehling, U. Onken, Vapor–Liquid Equilibrium Data Collection, Vol. 1, Part 2a, DECHEMA, Frankfurt, 1977.
[9] R.C. Reid, J.M. Prausnitz, B.E. Poling, The Properties of Gases and Liquids, 4th Edition, McGraw-Hill, New York, 1987.

[10] H. Kosuge, K. Asano, Mass and heat transfer in ternary distillation of methanol–ethanol–water systems by a wetted wall column, J. Chem. Eng. Jpn. 15 (1982) 268–273.
[11] AIChE Research Committee, Bubble Tray Design Manual, AIChE, New York, 1958.
[12] J. Stichlmair, Dimensionierung des gas/flussigkeit-kontaktapparates bodenkolonne, Chem. Ing. Tech. 50 (1978) 281–284, 383–387.
[13] H. Chan, J.R. Fair, Prediction of point efficiencies on sieve trays. I. Binary systems, Ind. Eng. Chem. Process. Des. Dev. 23 (1984) 814–819.
[14] F.J. Zuiderweg, Sieve trays: a view on the state of the art, Chem. Eng. Sci. 37 (1982) 1441–1464.
[15] R. Taylor, R. Krishna, Multicomponent Mass Transfer, 1st Edition, Wiley, New York, 1993, pp. 307–334.